Single Molecule Acid-Base Kinetics and Thermodynamics

Michael D. Mason, Krishanu Ray, and Robert D. Grober
Department of Applied Physics, Yale University, New Haven, Connecticut 06520, USA

Gerd Pohlers and James Cameron
Shipley Co., Marlborough, Massachusetts 01752, USA
(Received 26 February 2004; published 13 August 2004)

We report a method in which temperature dependent single-molecule fluorescence measurements are used to study the kinetics and thermodynamics of the acid-base interaction in films of photoresist polymer. We use the two distinct fluorescent prototropic forms of Coumarin 6 (C6 → C6 +) to indicate the state of the acid-base system. Data are analyzed using a statistical model of the intensity probability distributions, yielding temperature dependent proton exchange rates, which is confirmed through agreement with a simple two-state Monte Carlo model. The temperature dependent rates are used to calculate the activation enthalpy for proton exchange.

DOI: 10.1103/PhysRevLett.93.073004 PACS numbers: 33.50.–j, 33.15.–e

In recent years, there has been increasing interest in extending the capabilities of single-molecule techniques to include the ability to determine kinetic and thermodynamic quantities such as conformational exchange rates, free energies, and activation barriers [1–5]. Single-molecule imaging techniques enable optical measurements that probe materials on nanometer length scales. These techniques obviate the need to average over ensembles of fluorophores, making experiments particularly sensitive to dynamic and localized fluctuations. During the last decade, these methods have been applied to a variety of systems in both the biological and physical sciences [6,7] where the observation of static and dynamic disorder is of particular interest. One area, however, which has not been widely explored using these techniques, is the study of thin polymer film systems such as those used by the semiconductor industry for photolithography. A nanoscale understanding of the photolithographic process is of particular interest as desired feature sizes approach the molecular length scale.

It is currently believed that the photolithographic process is dominated by acid diffusion and as such considerable effort has gone into understanding this mechanism on the nanometer length scale [8]. Typical photolithographic processing requires the application of a post exposure bake (PEB), which is thought to initiate diffusion of the photo-acid to active sites within the polymer film [9]. The relative roles of thermal activation and acid diffusion during the development process are not well understood, however, and a detailed understanding of both diffusion and acid-base reaction kinetics in photoresist polymer systems is therefore of critical importance to the photolithography community [10].

In the method described in this text, we dope the *p*H sensitive fluorophore Coumarin 6 (C6) at nanomolar concentrations into a commercial photoresist polymer. The two prototropic forms of C6 exhibit unique absorption and emission energies allowing for their separation into two optical detection pathways in a confocal microscopic imaging technique [11]. The fluorophore, which acts as a competitive base, is shown to function as a noninvasive *in situ* probe of proton exchange kinetics within the polymer matrix where acid-base chemistry occurs.

Silsesquioxane based photoresist polymer films (~ 100 nm) were prepared on glass substrates containing nM concentrations of C6 and controlled quantities of trifluoroacetic acid, which was added instead of a typical photo-acid generator to control the acid concentration while obviating the need for UV exposure [12]. The concentration of trifluoroacetic acid was adjusted to achieve a *p*H of approximately 3.5, the equivalence point (pKa) of C6 in this polymer, comparable to acid concentrations used in commercial resist formulations. Fluorescence from the neutral and protonated forms of C6 molecules was imaged simultaneously in two channels using a home-built laser-scanning confocal microscope described in detail elsewhere [12]. Excitation of both species was accomplished using 457 and 532 nm laser lines. Leakage of neutral C6 emission into the protonated channel was eliminated by collecting a protonated signal out of phase with a chopper running at 2 kHz in the 457 nm excitation beam path [12]. In order to provide a sufficient signal-to-noise ratio, 2 μW laser excitation was used generating power densities of order 1 kW/cm^2 at the sample. For thin optically transparent samples, these power densities are not expected to dramatically affect the protonation or deprotonation process as a result of local heating. Integration times of 10 ms per pixel were used to obtain 128×128 pixel raster scanned 10×10 μm images. The resulting signal levels varied between 2 and 4 photons/ms/pixel with a typical noise floor of less than 1 photon/ms/pixel. Samples were mounted on a thermoelectric heater/cooler allowing the temperature of the samples to be varied from 10 to 80 °C (± 1 °C).

The two channel data are rendered as a single image by taking the ratio of the fluorescence intensities of the neutral and protonated channels ($R = I_n/I_p$) at each pixel. We have previously shown that R can be used to indicate the local pH of the system [12,13]. Because the samples are at the equilibrium point (i.e., pH = pKa), the data have been normalized such that the average value of R is equal to one. This corrects for differences in the emission and collection efficiencies between the neutral and protonated forms of C6. We do not observe a significant change in the absorption and emission properties of C6 over this temperature range (data not shown). As a result, the mean value of R, over a statistical ensemble of fluorophores, is very nearly invariant with temperature, indicating that the system remains in equilibrium throughout the range of temperatures used.

Images obtained at sample temperatures of 10, 50, and 80 °C are shown in Fig. 1 [(a), (b), and (c), respectively]. For the majority of the pixels in each image, the photon count rate in both channels is below the noise floor, which is determined from a detailed statistical analysis [12]. The pixels below this threshold are excluded from the analysis detailed below and are indicated as blue in the images of Fig. 1.

Diffraction limited spots corresponding to individual fluorophores are clearly evident in all three images. At 10 °C, the R-value images exhibit features that are generally either red ($R \ll 1$) or green ($R \gg 1$). We interpret this to mean that fluctuations between the neutral and protonated state of C6 take place on time scales longer than the acquisition time. When the sample is heated to temperatures around 50 °C, we see features with a broad range of behavior, including those that are fluctuating between red-orange and yellow-green and some that do not exhibit fluctuations in R. This suggests that fluctuations between neutral and protonated states occur on time scales comparable with the 10 ms/pixel acquisition rate. At 80 °C, most of the features exhibit a much narrower range of R values centered about $R = 1$, which is indicated as orange. Here the transition rates are clearly on time scales faster than the acquisition rate.

Each image pixel can be treated independently, thus discarding all spatial information, generating an ensemble of intensities. Intensity probability distributions are shown in Fig. 2 for samples at temperatures of 10, 50, and 80 °C. Each of these distributions represents an average over two types of sources: the fluorophore in a neutral state and the fluorophore in a protonated state. At the beginning of the acquisition of a pixel (i.e., at $t = 0$), there is a probability that the fluorophore could be in either the neutral or the protonated state, P_n and P_p, respectively. In general, if the local pH deviates significantly from the pKa of C6 in the film, then $P_n \neq P_p$ and the protonation and deprotonation rates differ. Because we have designed the experiment such that the pH of the sample is at the equivalence point (pKa) of the fluorophore, $P_n = P_p = 0.5$, it is assumed that the transition from a neutral to a protonated state occurs at the same rate, k, as the transition from a protonated to a neutral state. It is assumed that during the measurement period t, the number of transitions between states is distributed as a Poisson random variable with the average number of transitions equal to kt. A fluorophore that starts in the neutral state will be in the neutral state after time t with probability $P_{n,n}(t)$, which is given as the sum of the probability of all even numbers of transitions between states,

$$P_{n,n}(t) = \sum_{n=0,2,4,\ldots} \frac{(kt)^n}{n!} e^{-kt} = \frac{1}{2}(1 + e^{-2kt}). \qquad (1)$$

The probability that the fluorophore starts in the neutral state and after time t ends up in the protonated state is given as the sum of the probability of all odd numbers of transitions,

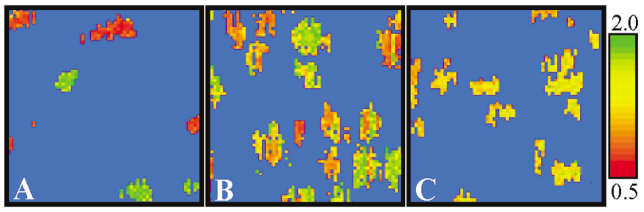

FIG. 1 (color). False-color scaled R-value images (5 × 5 μm) of C6 molecules in photoresist films (pH of the casting solution ~3.5) at 10 (a), 50 (b), and 80 °C (c). $R \ll 1$ (red), to $R = 1$ (orange), to $R \gg 1$ (green).

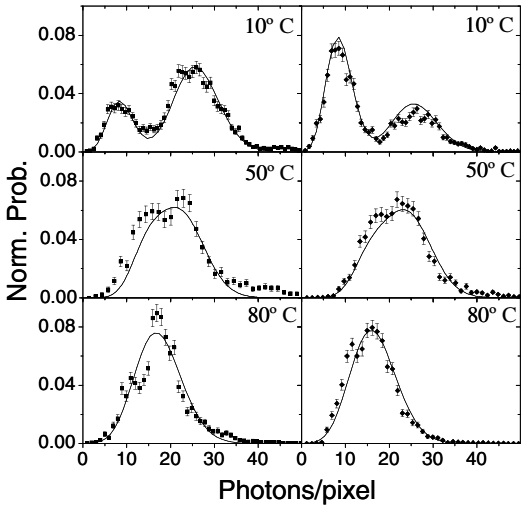

FIG. 2. Normalized intensity probability distributions for the neutral, P_n, (left panels) and protonated, P_p, (right panels) channels. Solid lines are fits to the experimental data points with Eqs. (7) and (8).

$$P_{p,n}(t) = \sum_{n=1,3,5,\ldots} \frac{(kt)^n}{n!} e^{-kt} = \frac{1}{2}(1 - e^{-2kt}). \quad (2)$$

Similarly, $P_{p,p}(t) = P_{n,n}(t)$ and $P_{p,n}(t) = P_{n,p}(t)$.

If a fluorophore starts in the neutral (protonated) state of C6 and emits photons at the rate I_n (I_p), then the average number of photons emitted in time τ from the neutral or protonated states, respectively, are given as

$$\mu_{n,n}(\tau) = \int_0^\tau P_{n,n}(t) I_n dt = \frac{I_n \tau}{2}\left(1 + \frac{1 - e^{-2k\tau}}{2k\tau}\right), \quad (3)$$

$$\mu_{n,p}(\tau) = \int_0^\tau P_{n,p}(t) I_n dt = \frac{I_n \tau}{2}\left(1 - \frac{1 - e^{-2k\tau}}{2k\tau}\right). \quad (4)$$

Similar expressions are obtained for the emission of photons from the protonated state:

$$\mu_{p,n}(\tau) = \frac{I_p \tau}{2}\left(1 - \frac{1 - e^{-2k\tau}}{2k\tau}\right); \quad (5)$$

$$\mu_{p,p}(\tau) = \frac{I_p \tau}{2}\left(1 + \frac{1 - e^{-2k\tau}}{2k\tau}\right). \quad (6)$$

In practice, all of these expressions must be adjusted to account for the background noise of the experiments. We have measured the background for each channel and label it as $\mu_{n,B}(\tau)$ for the background in the neutral channel and $\mu_{p,B}(\tau)$ for the background in the protonated channel [14]. These are then added to the expressions of Eqs. (3) and (4) and Eqs. (5) and (6), respectively.

Consider now the case of detection in the neutral channel. If the fluorophore under study starts in the neutral state, the detected intensity will be Poisson distributed about the mean $\mu_{n,n}(\tau)$. This Poisson distribution is $\xi(I, \mu) = (\mu^I/I!)e^{-\mu}$, where I is the number of photons detected, and μ is the average number of photons detected.

The probabilities of measuring I_n or I_p photons in the neutral or protonated channels in measurement period τ are

$$P(I_n, \tau) = P_n \xi(I_n, \mu_{n,n}(\tau)) + P_p \xi(I_n, \mu_{n,p}(\tau)), \quad (7)$$

$$P(I_p, \tau) = P_n \xi(I_p, \mu_{p,n}(\tau)) + P_p \xi(I_p, \mu_{p,p}(\tau)). \quad (8)$$

The solid lines in Fig. 2 are best fits of Eqs. (7) and (8) to the data. I_n and I_p are obtained directly from the data and have values ranging from 2.5–5 kHz. Once I_n and I_p are fixed, the only free parameter in the fit is k, the transition rate. The rates obtained are 75 ± 7, 252 ± 19, and 580 ± 95 Hz for 10, 50, and 80 °C, respectively.

While the above analysis demonstrates that we understand the measured intensity probability distributions, it does not address the correlations between the two states of C6. We model this effect with a relatively simple kinetic Monte Carlo model [15]. An advantage of the Monte Carlo model is that it can more accurately account for experimental details. For instance, the simulated signal is convolved with a two-dimensional Gaussian to account for the intensity distribution of the excitation profile. Monte Carlo simulation uses the parameters determined from the analytical model described above. As is shown in Fig. 3(a), the Monte Carlo model yields the correct probability distributions.

The correlation between signal channels is represented as distributions of R values in Fig. 3(b). The histograms shown in the left panels are experimental data taken at the temperatures 10, 50, and 80 °C. The histograms shown in the right panels are simulated data generated by the Monte Carlo calculation. The excellent agreement between the real and simulated R-value histograms and the probability distributions demonstrate the validity of the calculated rate parameters. Furthermore, the ratio of the relative areas of each population [Fig. 3(b)] is approximately constant, indicating that the ensemble pH does

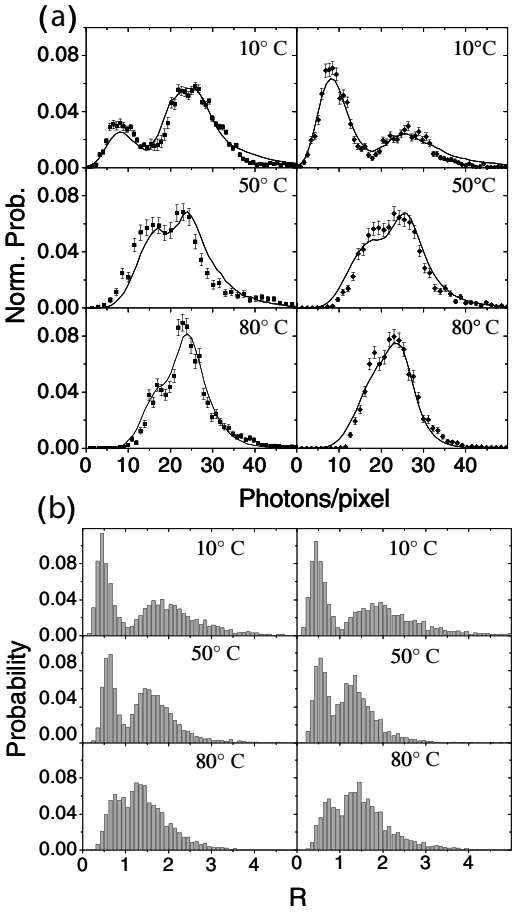

FIG. 3. (a) Normalized intensity probability distributions of P_n (left panels) and P_p (right panels). Monte Carlo simulations are shown as a solid line superimposed over the data. (b) Histograms of $R = I_n/I_p$ obtained from the C6 image data (left panels) and simulated image data (right panels).

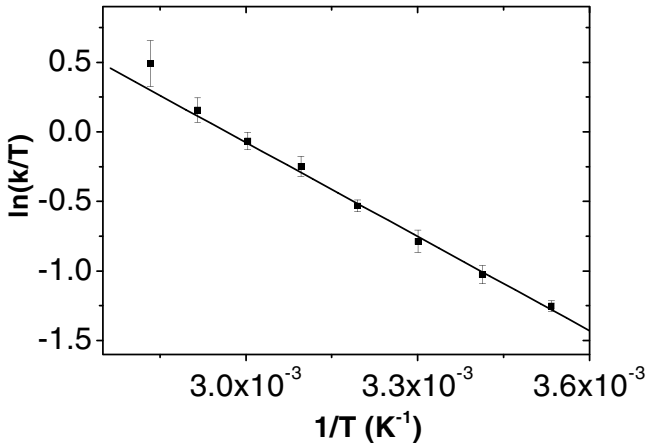

FIG. 4. Plot of $\ln(k/T)$ versus $1/T$ and subsequent fit according to the Eyring equation.

not change significantly over the temperature range used here.

The measurements and analyses described above have been performed at eight temperatures between 10 and 80 °C. Shown in Fig. 4 are the resulting proton exchange rates plotted versus $1/T$ on a log-linear plot. The data fit well to a straight line. This is consistent with the Eyring equation, $\ln(k/T) = C - \Delta H/RT$, from which we determine the activation enthalpy, $\Delta H = 4.5 \pm 0.2$ kcal/mol. This number is somewhat lower than the 7.85 kcal/mol value previously measured on a similar thin film polymer obtained using temperature dependent IR spectroscopy [10]. Proton exchange rates and activation enthalpies for nonaqueous, nonpolymer solutions have been reported as 10^6–10^{12} s^{-1} and 0.1–10 kcal/mol, respectively [16]. The slower rates we measure here, relative to those in solution, should not be too surprising as proton exchange, and exchange in general, involves a reorganization of the local matrix. This requires the polymer to physically move to adjust to the new charge arrangement, which can require considerable energy.

The PEB temperature used in the processing of photoresists is of order T_g, the glass transition temperature of the polymer. We have measured the protonation rate constant to be 580 Hz at 80 °C, which is very close to the Tg (84 °C) of the polymer studied in this experiment. This rate can be compared with the relevant acid diffusion time constants to determine the relative importance of diffusion and protonation kinetics in the lithographic process. For the sake of argument, we assume $D = 1 \times 10^{-14}$ cm^2/s [17]. The relevant length is the size scale of the typical polymer, $L \sim 1$ nm. Thus one estimates the diffusion limited time between subsequent catalytic events to be of order $\tau = L^2/D = 1$ s. This estimate suggests that the extremely slow protonation kinetics reported in this Letter do not limit the PEB chemistry; rather, still slower diffusive processes limit PEB. However, it is worth cautioning that the values of diffusion constants reported in the literature vary over many orders of magnitude [9,10] and are expected to be much faster for small acids. It is likely that for diffusion constants larger than 10^{-11} cm^2/s the protonation kinetics become the rate limiting reaction in the PEB process.

This work demonstrates that the proton exchange rates in thin solid films can be obtained using two color single-molecule imaging spectroscopy. The experimental data have been interpreted with an analytical model and verified with Monte Carlo simulation, yielding temperature dependent proton exchange rates that vary from 75 to 580 Hz as the temperature is varied from 10 to 80 °C. These rates are surprisingly slow, especially when compared to protonation kinetics in solution. While it is our best guess that these relatively slow protonation kinetics are faster than the acid diffusion processes which are thought to limit the reaction rates during the post exposure bake, this may not be generically true for all photoresists and warrants further study.

Support was provided by the Semiconductor Research Corp. and NSF under Grant No. 0211422.

[1] X. S. Xie and J. K. Trautman, Annu. Rev. Phys. Chem. **49**, 441 (1998).
[2] S. Weiss, Nat. Struct. Biol. **7**, 724 (2000).
[3] Y. J. Jung, E. Barkai, and R. J. Silbey, J. Chem. Phys. **117**, 10 980 (2002).
[4] I. Tinoco, Jr. and C. Bustamante, Biophys. Chem. **101**, 513 (2002).
[5] A. M. van Oijen *et al.*, Science **301**, 1235 (2003).
[6] W. E. Moerner, J. Phys. Chem. B **106**, 910 (2002).
[7] L. A. Deschenes and D. A. Vanden Bout, Science **292**, 255 (2001).
[8] E. K. Lin *et al.*, Science **297**, 372 (2002).
[9] G. M. Wallraff and W. D. Hinsberg, Chem. Rev. **99**, 1801 (1999).
[10] F. A. Houle *et al.*, J. Vac. Sci. Technol. B **18**, 1874 (2000).
[11] L. Edman *et al.*, Chem. Phys. Lett. **292**, 15 (1998).
[12] M. D. Mason *et al.*, J. Phys. Chem. B **107**, 14 219 (2003).
[13] S. Brasselet and W. E. Moerner, Single Mol. **1**, 17 (2000).
[14] The average background levels for each image (μ_{nB}, μ_{pB}) are obtained iteratively by calculating μ, cropping all features above $\mu + 2\sqrt{\mu}$, recalculating μ, and so on.
[15] The model consists of three manifolds: C6 (states 1, 2), C6+ (states 3, 4), and a dark manifold (states 5, 6) which includes dark counts as well as triplet dynamics. The forward and reverse proton exchange rates, which are equivalent when $p\mathrm{H} = \mathrm{pKa}$ ($k = k_{13}, k_{31}$), and background levels are used to generate conditional transition probabilities between states, which, in turn, dictate the final state of each random event.
[16] K. S. Peters and G. Kim, J. Phys. Chem. A **105**, 4177 (2001).
[17] M. D. Stewart *et al.*, J. Vac. Sci. Technol. B **20**, 2946 (2002).